Title:
Dot Grid Detection and Tracking for Sheet Metal Strain Analysis

Authors:
Tyler Kenyon, kenyot@mcmaster.ca, McMaster University
Allan Spence, adspence@mcmaster.ca, McMaster University
David Capson, capson@uvic.ca, University of Victoria

Keywords:
Computer vision, feature detection, strain analysis, fiducial tracking

DOI: 10.14733/cadconfP.2015.349-353

Introduction:
A substantial fraction of the automotive assembly comprises formed sheet metal parts. To reduce vehicle weight and improve fuel economy, total sheet metal mass should be minimized without compromising the structural integrity of the vehicle. Excessive deformation during manufacture contributes to tearing or wrinkling of the metal, and therefore a forming limit is investigated experimentally to determine the extent to which each particular material can be safely strained. To assess sheet metal formability, this paper investigates sheet metal surface strain measurement using a scalable dot grid pattern. Aluminum sheet metal samples are marked with a regular grid of dot features and imaged with a close-range monocular vision system. After forming, the samples are imaged once again to examine the deformation of the surface pattern, and thereby resolve the material strain. Grid features are localized with sub-pixel accuracy, and then topologically mapped using a novel algorithm for deformation invariant grid registration. Experimental results collected from a laboratory setup demonstrate consistent robustness under practical imaging conditions. Representative accuracy, repeatability, and timing statistics are reported for the SURF feature detector.

Main Idea:
Material Forming Limit Tests
Each sheet metal material possesses certain characteristics that determine the forming strain limits (Fig. 1(a)). Experimentally, these are commonly measured using a die/blank holder and punch that deforms initially flat test material into a dome (Fig. 1(b)). By etching or printing a regularly spaced grid onto the flat material, the surface strain after forming can be measured, and the resulting thickness strain ε_3 derived (Fig. 1(c)).

Every material has two surface strains ε_1 (major) and ε_2 (minor). When both strains are positive (tension), the material can be stretched until it cracks. When the minor strain is negative (compression), the material can be drawn until the strain Forming Limit is exceeded and either wrinkles or cracks appear (Fig. 1(d)). The strain may be measured by finding three grid element vertices and establishing a local (undeformed) triangle AOB (Fig. 1(e)). After forming, the distorted vertices form the triangle $A'OB'$. The coordinates distort from $A\ X_A,Y_A$ and $B\ X_B,Y_B$ to $A'\ x_{A'},y_{A'}$ and $B'\ x_{B'},y_{B'}$. Using a 2×2 strain gradient tensor $\mathbf{F}$, this distortion can be expressed using the linear system

$$\begin{bmatrix} x_{A'} \\ y_{A'} \end{bmatrix} = \begin{bmatrix} F_{11} & F_{12} \\ F_{21} & F_{22} \end{bmatrix} \cdot \begin{bmatrix} X_A \\ Y_A \end{bmatrix}, \quad \begin{bmatrix} x_{B'} \\ y_{B'} \end{bmatrix} = \begin{bmatrix} F_{11} & F_{12} \\ F_{21} & F_{22} \end{bmatrix} \cdot \begin{bmatrix} X_B \\ Y_B \end{bmatrix}$$

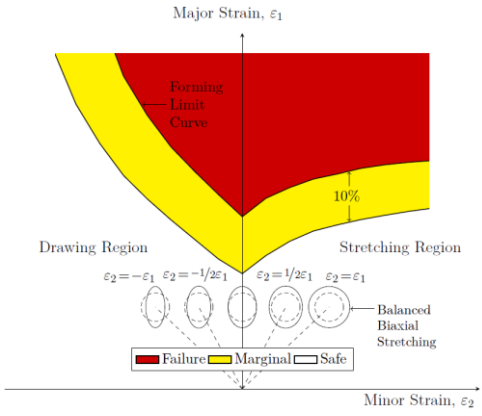

(a)

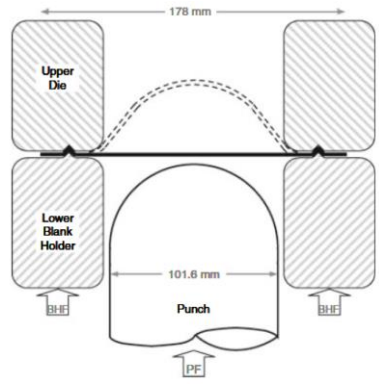

(b)

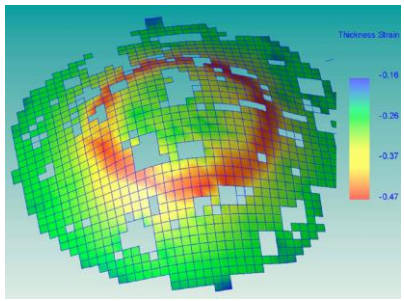

(c)

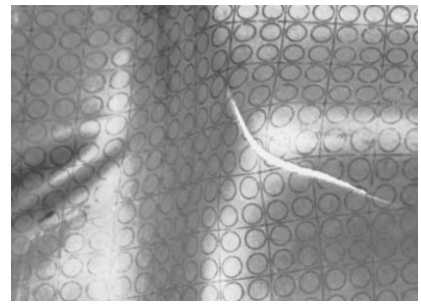

(d)

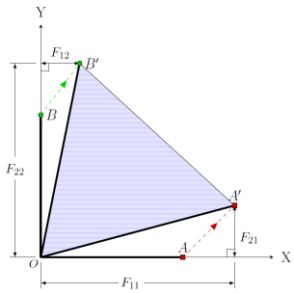

(e)

(f)

Fig. 1: (a) Forming Limit Diagram [1], (b) Die/Blank Holder and Punch Experimental Setup [2], (c) Derived Material Thickness plot [3], (d) Wrinkles and Cracks when Forming Limit Exceeded, (e) Grid Element Strain Mathematics [4], (f) Dot Gridded Sheet Metal (after deformation).

After rearranging

$$\begin{bmatrix} x_{A'} \\ x_{B'} \\ y_{A'} \\ y_{B'} \end{bmatrix} = \begin{bmatrix} X_A & Y_A & 0 & 0 \\ X_B & Y_B & 0 & 0 \\ 0 & 0 & X_A & Y_A \\ 0 & 0 & X_B & Y_B \end{bmatrix} \cdot \begin{bmatrix} F_{11} \\ F_{12} \\ F_{21} \\ F_{22} \end{bmatrix}$$

can be solved for $\mathbf{F}$. The strains are $\varepsilon_{1,2} = \ln \lambda_{1,2}$ where $\lambda_{1,2}$ are the eigenvalues of $\mathbf{F}$. Because the material volume does not change, the third thickness strain is computed as $\varepsilon_3 = -\varepsilon_1 - \varepsilon_2$.

The remaining practical issues are to: i) print the grid onto the flat sheet metal; and ii) accurately detect the grid vertices.

Dot Grid Printing

In order to obtain high accuracy, close-up computer vision, in which only a small portion of the sheet metal surface will be available in any one video frame is used. Hence some means of introducing fiducials into the regular grid pattern is needed. After investigation, the chosen method was to use an inkjet printer (Roland VersaUV LEJ-640). This printer features a 4 foot by 8 foot flat bed, and 1440 by 1440 dot per inch resolution. The ink is ultraviolet light cured for rapid drying, and can stretch up to 220 percent. To avoid any tearing, individual 0.028 inch diameter black dots were printed on 0.040 inch centers. Occasional dots were omitted to provide fiducials for close-up camera tracking (Fig. 1(f)).

Grid Vertex Detection

The computer vision camera was a Point Grey Research Dragonfly with 1024 by 768 pixels and 8 bit grey level per pixel operated at 15 frames per second. A 1 mm extension ring was used to obtain a close-up object to sensor distance. To locate the dots, several feature detectors were investigated first using synthetic methods, and also with the actual camera and gridded sheet metal [5]. The Speeded-Up Robust Features (SURF) algorithm [6] provided the best performance, with speed exceeding 20 frames per second (2.8 GHz Intel i7), and local error less than 0.25 pixels. Over 99 percent of all dot features were detected (Fig. 2(a,b)). Fundamentally, the SURF computation uses an approximation of the determinant of the Hessian

$$\det H_{\text{approx}} = D_{xx}D_{yy} + wD_{xy}^{2}$$

where D_{xx}, D_{yy}, and D_{xy} denote box convolution filters that approximate the second order Gaussian derivatives (Fig. 2(c)) and w is an experimentally determined balancing weight. To enable fast computation of the box convolution filters, integral images [7] are used. False positives are eliminated using non-maximum suppression [8] in a 3 by 3 by 3 neighborhood, and the feature is localized to sub-pixel resolution.

The features were then connected using a topological nearest neighbor graph and breadth first search (Fig. 3(a)) [9]. Interframe video tracking was accomplished by assigning regular (dot present) nodes a fiducial metric value of $\sigma = 1$. Omitted dots are assigned the extreme metric value $\sigma = 100$. Because grid directions are carried forward from frame to frame, overlay grid matching from the previous to current frame involves only horizontal/vertical discrete shifts. The objective function used was

$$F\ i,j\ = \sum_{\substack{x,y\ \in G^{k} \\ x+i,y+j\ \in G^{k-1}}} \sigma_{x,y}^{k} - \sigma_{x+1,y+j}^{k-1}{}^{2} + P\ i,j$$

where i,j is the interframe shift and x,y denote the location of the node within the k th grid frame G^{k}. The grid shift term $P\ i,j\ = \sqrt{i^2 + j^2}$ penalizes large changes from frame to frame. The typical result contains a very distinct minimum (Fig. 3(b)). The sweeping motion chronological evolution of feature detection is illustrated in Fig. 3(c), where the frame in which each dot feature is first detected is plotted.

Conclusions:

This paper uses inkjet printer-based dot grids as features to be measured for sheet metal strain analysis. The SURF feature algorithm provided excellent detection coverage and fractional pixel error. By creating a topological map, and occasionally omitting dots, a fiducial was achieved that, when combined with a practical objective function very distinctly identifies the interframe motion, even under very close-up conditions.

Acknowledgements:
Financial support for this work was received from a Natural Sciences and Engineering Research Council of Canada (NSERC) Discovery Grant. Inkjet printing was performed at Mohawk College (Hamilton, ON, Canada). The sheet metal was provided by Mukesh Jain, and forming services were provided by Mike Bruhis.

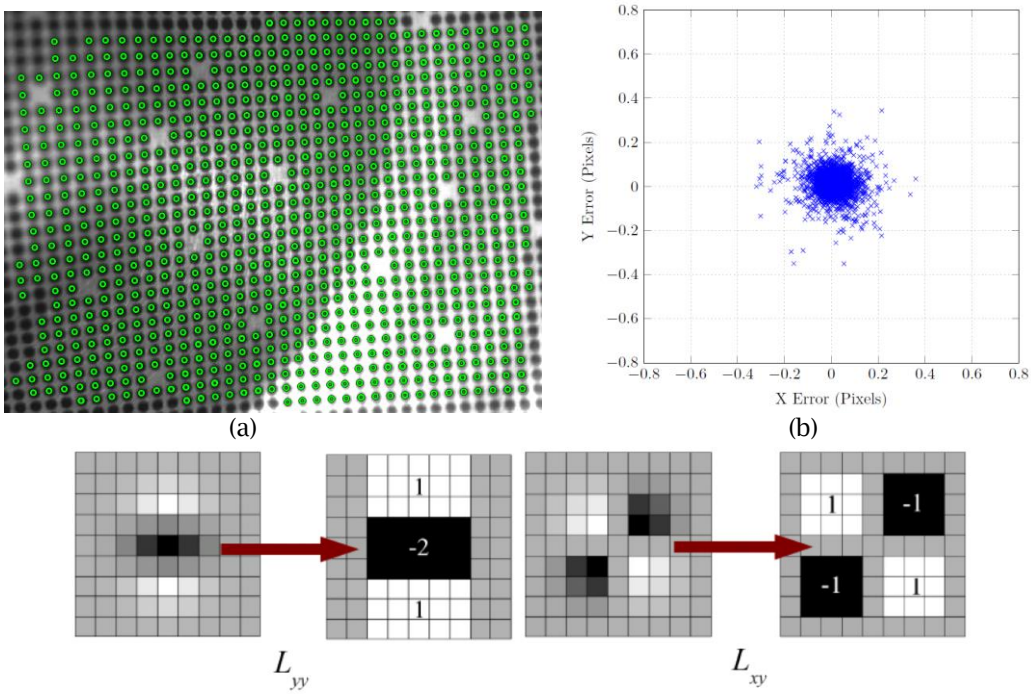

Fig. 2: (a) SURF Feature Detector Performance on Actual Printed and Formed Dome, (b) Local Pixel Error Plot, (c) Box Convolution Filter.

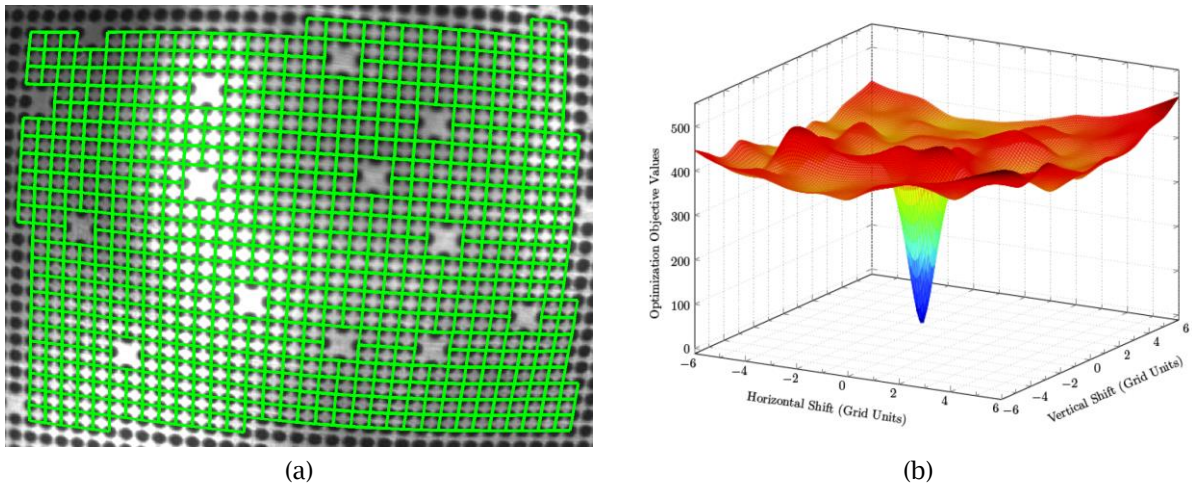

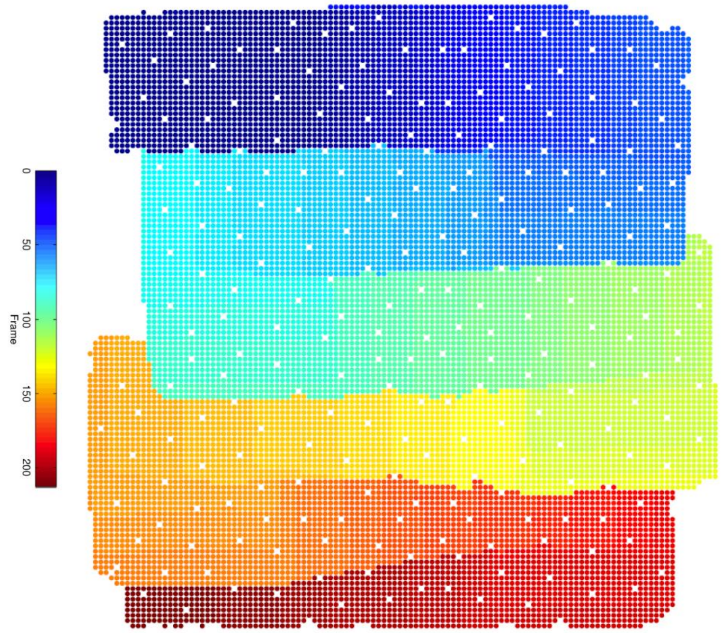

(c)

Fig. 3: (a) Topological Node Map; (b) Sample Objective Function Plot; (c) Chronological Plot of Frame in which Feature is First Detected.

References:

[1] Chan, H.-L.; Spence, A.; Sklad, M.: Laser digitizer-based sheet metal strain and surface analysis. International Journal of Machine Tools and Manufacture, 47(1), 2007, 191-203. http://dx.doi.org/10.1016/j.ijmachtools.2005.12.013

[2] Hsu, E.; Carsley, J.E.; Verma, R.: Development of forming limit diagrams of aluminum and magnesium sheet alloys at elevated temperatures, Journal of Materials Engineering and Performance, 17(3), 2008, 288-296. http://dx.doi.org/10.1007/s11665-007-9196-y

[3] Spence, A.D.; Capson, D.W.; Sklad, M.P.; Chan, H.-L.; Mitchell, J.P., Simultaneous large scale sheet metal geometry and strain measurement, ASME Journal of Manufacturing Science and Engineering, 130(5), 2008, paper 054502. http://dx.doi.org/10.1115/1.2976121

[4] Sowerby, R.; Duncan, J.; Chu, E.: The modelling of sheet metal stampings, International Journal of Mechanical Sciences, 28(7), 1986, 415-430, http://dx.doi.org/10.1016/0020-7403(86)90062-7

[5] Kenyon, T.: Close-Range Machine Vision for Strain Analysis, Master's thesis, 2014, McMaster University, http://hdl.handle.net/11375/16324

[6] Bay, H.; Ess, A.; Tuytelaars, T.; Van Gool, L.: Speeded-up robust features (SURF), Computer Vision and Image Understanding, 110(3), 2008, 346-359. http://dx.doi.org/10.1016/j.cviu.2007.09.014

[7] Viola, P.; Jones, M.J.: Robust real-time face detection, International Journal of Computer Vision, 57(2), 2004, 137-154. http://dx.doi.org/10.1023/B:VISI.0000013087.49260.fb

[8] Neubeck, A.; Van Gool, L.: Efficient non-maximum suppression, 18th International Conference on Pattern Recognition, 3(c), Hong Kong, Aug. 20-24, 2006, 850-855. http://dx.doi.org/10.1109/ICPR.2006.479

[9] Kinsner, M.H.; Kenyon, T.; Capson, D.W.; Spence, A.D.: Multiple View Motion Tracking of Gridded Surfaces using Topological Structure, Computer-Aided Design and Applications, 10(2), 2013, 221-229. http://dx.doi.org/10.3722/cadaps.2013.221-229